3-4

Monte Carlo simulation of 50nm devices with Schottky contact model

K. Matsuzawa, K. Uchida, and A. Nishiyama

Advanced LSI Technology Laboratory, Toshiba Corporation
8, Shinsugita-cho, Isogo-ku, Yokohama 235-8522, Japan
Phone: +81-45-770-3693, Fax: +81-45-770-3578,
E-mail: kazuya.matsuzawa@toshiba.co.jp

Abstract A Schottky contact model was implemented as a boundary condition for a Monte Carlo device simulation. Unlike the ideal ohmic contact, thermal equilibrium is unnecessary around the Schottky contact. Therefore, the wide region of high impurity concentration around contacts is not required to maintain the thermal equilibrium, which means that it is possible to avoid assigning a lot of particles to the low-field region. The validity of the present boundary condition for contacts was verified by simulating a rectifying characteristic of a Schottky barrier diode. As an application example of the present boundary condition, we simulated the transport in n^+nn^+ structures with sub-0.1 μm channel length. We found direction dependence of the electron velocity dispersion, which indicates that the direction dependence of the diffusion constant or the carrier temperature should be taken into account in the hydrodynamic simulation for sub-0.1 μm devices.

1. Introduction

The Monte Carlo method has been utilized to reveal the transport characteristics in sub-0.1 μm devices [1][2]. One of the important issues in Monte Carlo device simulations is the treatment of the boundary condition at contacts [3]. In many cases, the number of particles around contacts is fixed to assure the charge neutrality under the assumption of the ideal ohmic contact in equilibrium. Hence, a wide region with high impurity concentration is required to keep the equilibrium condition around contacts. Therefore, a lot of particles must be assigned to the low-field region, resulting in lack of particles in the high-field region, where the Monte Carlo method is vital. Moreover, the neutral charge condition cannot be applied to contacts attached to a high resistive region.

In this work, a Schottky contact model was implemented in our Monte Carlo device simulator. Particles were eliminated and supplied by thermionic emission just at the metal/semiconductor interface and the tunneling around the interface. The ohmic contact is a special case of the Schottky contact, in which the tunneling probability is quite high. Using the Schottky contact model makes it possible to carry out Monte Carlo device simulations without the wide region of high impurity concentration, since the thermal equilibrium and neutral charge conditions are unnecessary around the Schottky contact. Moreover, the influence of the contact resistance can naturally be included in Monte Carlo device simulations. The nature of the Schottky contact has been studied by using the Monte Carlo method [4][5][6]. However, the Schottky contact has not been utilized as the boundary condition in simulations of usual devices. The validity of the present boundary condition was checked by comparing a rectifying characteristic of an SBD (Schottky barrier diode) with that obtained by the drift diffusion with a similar Schottky contact model [7]. Using the present boundary condition for simulations of n^+nn^+ structures, fundamental characteristics of transport in sub-0.1 μm lengths were investigated.

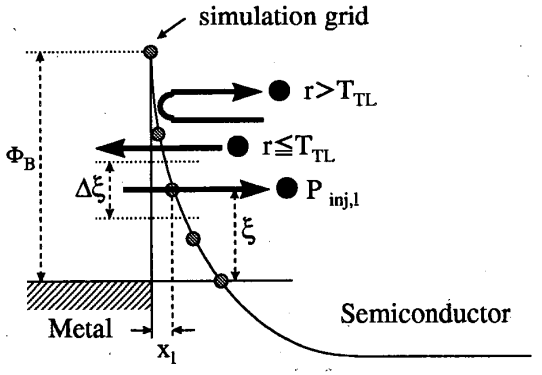

Figure 1: Schematic band diagram around the interface between metal and semiconductor to show behavior of particles.

2. Schottky contact model

The tunneling probability T_{TL} was calculated based on the WKB approximation and a triangle potential around contacts:

$$T_{TL}(\xi) = exp\left(-\frac{4\sqrt{2m^*}(\xi_0-\xi)^{1.5}}{3\hbar q|E|}\right), \quad (1)$$

$$\xi = -q\psi, \quad (2)$$

$$\xi_0 = -q\psi_0, \quad (3)$$

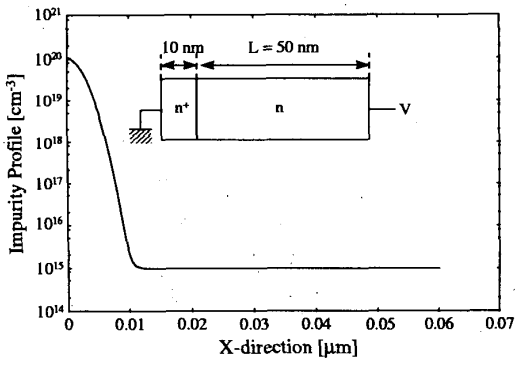

Figure 2: Schematic of Schottky barrier diode and the impurity concentration profile.

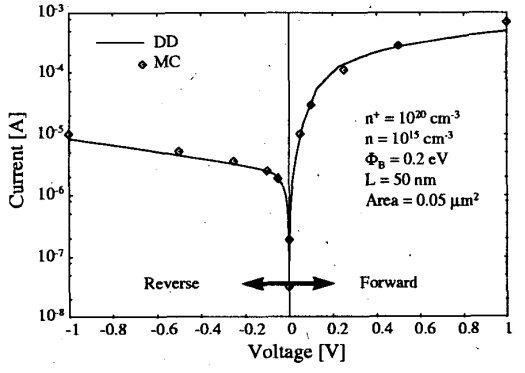

Figure 3: Rectifying characteristics of Schottky barrier diode.

$$E = -\frac{\psi - \psi_0}{x_l}, \tag{4}$$

where ξ is the electron energy, m^* the effective mass ($0.26m_0$ for electrons in silicon, m_0 the electron rest mass), ξ_0 the electron energy at the interface, $\hbar$ the reduced Planck constant, q the elementary charge, E the average electric field, ψ the potential at each grid, ψ_0 the potential at the interface, and x_l the distance from the interface. A random number r, uniformly distributed between 0 and 1, is generated for a particle reaching the turning point, namely, whose energy parallel to its tunneling path becomes zero. Then, the particle is absorbed if $r \leq T_{TL}$, or reflected if $r > T_{TL}$, as shown schematically in Fig. 1 [8]. Particles reaching the interface of semiconductor and metal are perfectly absorbed, which corresponds to the thermionic emission.

On the other hand, particles are injected from the metal contact according to the probability $P_{inj,l}$ at each control volume l:

$$P_{inj,l} = \frac{A}{q} T^2 T_{TL}(\xi) f_M(\xi) \frac{\Delta\xi}{k_B T} S, \tag{5}$$

$$\xi_f = \xi_0 - q\phi_B, \tag{6}$$

where A [$\mathrm{Acm^{-2}K^{-2}}$] is the Richardson constant (112 for electrons in silicon [9]), T the electron temperature, f_M the energy distribution function in the metal, $\Delta\xi$ the energy difference in the control volume specified by discretization grids, k_B Boltzmann's constant, S the cross-sectional area of the control volume perpendicular to the tunneling path, ξ_f the Fermi level used in f_M, and ϕ_B the barrier height. $T_{TL} = 1$ just at the metal/semiconductor interface. Time interval of injection and the injection point are determined according to $P_{inj,l}$ in a similar manner to that for the scattering process [10]. Namely, particles are injected with the time interval of δt calculated by

$$\delta t = -\frac{ln(r)}{\Gamma}, \tag{7}$$

$$\Gamma = \sum_l P_{inj,l}. \tag{8}$$

The injection point x_l is selected when the following condition is satisfied:

$$\sum_{k=1}^{l-1} \frac{P_{inj,k}}{\Gamma} \leq r < \sum_{k=1}^{l} \frac{P_{inj,k}}{\Gamma}. \tag{9}$$

In the present simulations, the Poisson equation was solved every 1 [fs] and the potential distribution and the tunneling probability were calculated self-consistently. Simulation was carried out until 100 [ps], and results averaged over a period from 30 to 100 [ps]. The spherical band model was used for clear extraction of the direction dependence of the velocity dispersion discussed in the following section.

An SBD shown in Fig. 2 was simulated using the present contact model. The cathode and anode were Schottky contacts with $\phi_B = 0.2$ [eV]. Figure 3 shows a rectifying characteristic of the SBD. Under reverse biases, currents are suppressed by low tunneling probability at the anode contact, whereas currents under forward biases show the ohmic nature due to the high probability of tunneling at the cathode contact. At the zero bias, the total current is sufficiently low, which means that the balance between inflow and outflow at the interface of metal and semiconductor is maintained and the Richardson constant for electrons is adequate. Good agreement with results of a drift-diffusion model was obtained as shown in Fig. 3. It has been shown that the drift-diffusion simulation with the Schottky contact model reproduced measurements of SBDs [7]. Therefore, the present model provides the appropriate boundary condition for the Monte Carlo device simulation.

3. Simulations of n^+nn^+ structures

A simple n^+nn^+ structure shown in Fig. 4 was analyzed to interpret the fundamental characteristics of transport in the sub-0.1 μm length. The barrier height of the cathode and anode contacts was $\phi_B = 0.2$ [eV]. Figure 5 shows the potential and electron energy distributions. The shape of the potential distribution around contacts reflects the Schottky barrier, which is unlike that around the conventional ohmic contact boundary.

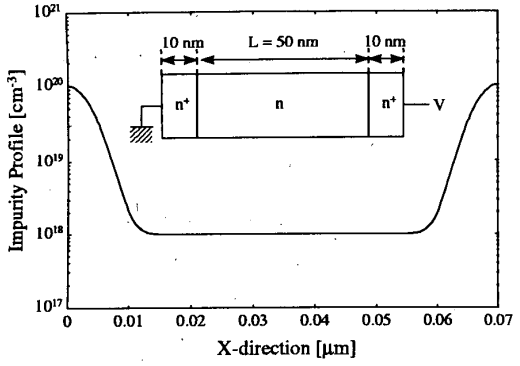

Figure 4: Schematic of n^+nn^+ structure and the impurity concentration profile.

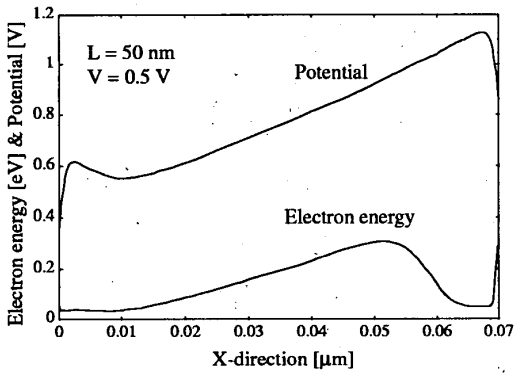

Figure 5: Potential and energy distributions in n^+nn^+ with L = 50 nm.

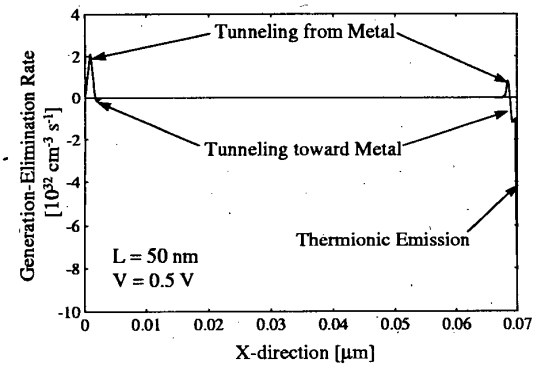

Figure 6: Generation and elimination distribution in n^+nn^+ with L = 50 nm.

Figure 6 shows the distribution of generation and elimination rates. Positive values indicate the generation rate of electrons supplied by the thermionic emission and the tunneling from contacts, whereas negative values indicate the elimination rate of electrons absorbed by contacts. Tunneling peaks from contacts appear at positions corresponding to energy higher than the Fermi level in metal, because the temperature was 300 [K].

Figure 7 shows the velocity dispersion of each direction, σ_{vx}^2, σ_{vz}^2, and the average dispersion of all directions, σ_v^2 for L = 50 nm, calculated by the following equations:

$$\sigma_{vx}^2 = < v_x^2 > - < v_x >^2 = \frac{k_B T_x}{m^*}, \quad (10)$$

$$\sigma_{vz}^2 = < v_z^2 > - < v_z >^2 = \frac{k_B T_z}{m^*}, \quad (11)$$

$$\sigma_v^2 = \frac{< \vec{v}^2 > - < \vec{v} >^2}{3} = \frac{k_B T}{m^*}, \quad (12)$$

where v_x and v_z are the velocities of the x- and z-directions, and $\vec{v}$ is the velocity vector. For the vertical directions, σ_{vy}^2 is the same as σ_{vz}^2, therefore only σ_{vz}^2 is shown. The direction dependence of the velocity dispersion can be observed in spite of the assumption of the spherical energy band. The direction dependence near the cathode is caused by the cooling of electrons, whose x-direction energy is decreased by the retarding field at the cathode junction, whereas the general energy tends to relax from cooled energy to the value corresponding to the lattice temperature by phonon scattering. Therefore, σ_{vz}^2 increases through energy emitted by the phonon.

On the other hand, the direction dependence near the anode is caused by the quasi-ballistic transport. Although σ_{vx}^2 increases by acceleration and scattering, the time and space are insufficient for propagation of the dispersion from the x-direction to the z-direction. Indeed, the direction dependence of velocity dispersion for L = 0.1 μm decreases as shown in Fig. 8, compared with that for L = 50 nm. This is because the randomization of the velocity progresses by scattering. On the contrary, Fig. 9 shows that the direction dependence increases for L = 25 nm.

Figure 10 shows the distribution of the velocity dispersion normalized by the average dispersion. It was found that the direction dependence caused by cooling around the cathode junction does not depend on the channel length, whereas the direction dependence caused by the quasi-ballistic transport near the anode decreases as the channel length becomes longer. Consequently, the direction dependence should be included in the diffusion constant or the carrier temperature in the hydrodynamic simulation for sub-0.1 μm devices.

4. Conclusions

The Schottky contact model was implemented in the Monte Carlo device simulation, which allowed the simulation to be performed without the restriction of the equilibrium condition around contacts. As the application example, the simple n^+nn^+ structures were simulated.

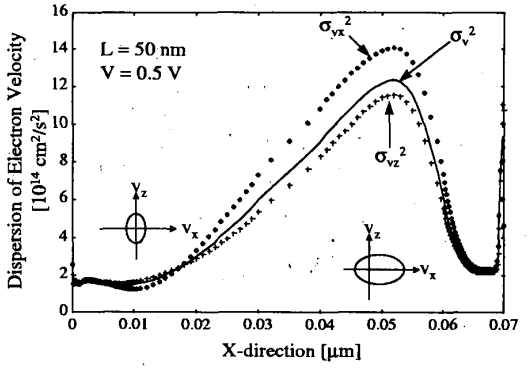

Figure 7: The distribution of the velocity dispersion in n^+nn^+ structure with a channel length of 50 nm.

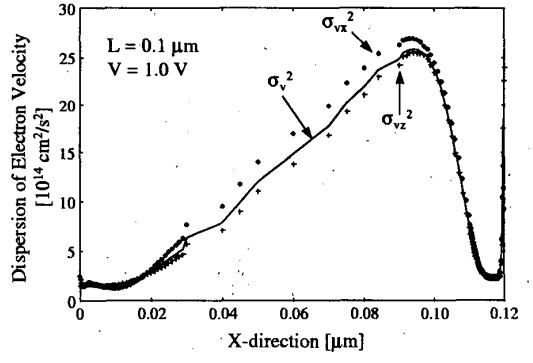

Figure 8: The distribution of the velocity dispersion in n^+nn^+ structure with a channel length of 0.1 μm.

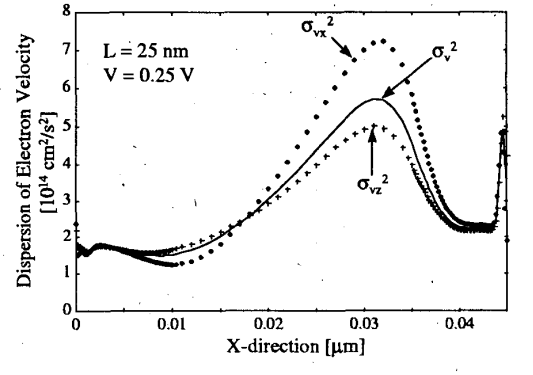

Figure 9: The distribution of the velocity dispersion in n^+nn^+ structure with a channel length of 25 nm.

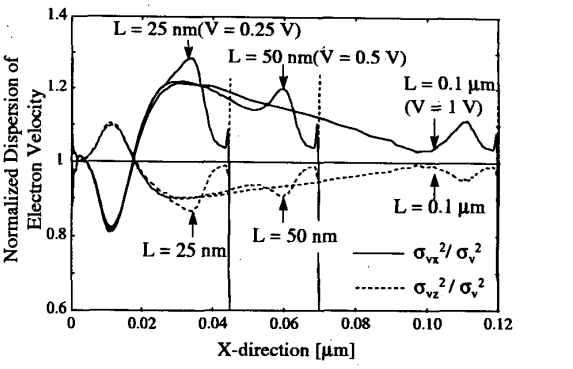

Figure 10: The distribution of the velocity dispersion normalized by the averaged dispersion in n^+nn^+ structures with channel lengths of 25nm, 50nm, and 0.1 μm.

The significant direction dependence of the velocity dispersion was observed for the sub-0.1 μm channel length, which indicates that the direction dependence of the diffusion constant or carrier temperature should be taken into account in the hydrodynamic model for sub-0.1 μm devices.

Acknowledgment

The authors wish to thank Mr. Oowaki, Dr. Takagi, and Dr. Toriumi for their valuable comments.

References

[1] N. Sano, K. Natori, M. Mukai, and K. Matsuzawa, IWCE-6, p. 112, 1998.

[2] D. J. Frank, S. E. Laux and M. V. Fischetti, in IEDM Tech. Dig., p.553, 1992.

[3] D. L. Woolard, H. Tian, M. A. Littlejohn, and K. W. Kim, IEEE Trans. Computer-Aided Design, vol.13, p.1241, 1994.

[4] M. J. Martin, T. Gonzalez, D. Pardo, and J. E. Velazquez, Semicond. Sci. Technol. vol, 11, p. 380, 1996.

[5] R. E. Lipsey, S. H. Jones, J. R. Jones, T. W. Crowe, L. F. Horvath, U. V. Bhapkar, and R. J. Mattauch, IEEE Trans. Electron Devices, vol. 44, p. 1843, 1997.

[6] J. East and P. Blakey, Proc. IEEE/Cornell Conference on Advanced Concepts in High Speed Semiconductor Devices and Circuits, 406, P. 59, 1997.

[7] K. Matsuzawa, K. Uchida, and A. Nishiyama, IWCE-6, p. 163, 1998.

[8] P. Lugli, U. Ravaioli, and D. K. Ferry, AIP Conf. Proc., no. 122, p. 162, 1984.

[9] J. M. Andrews and M. P. Lepselter, Solid-State Electron., vol. 13, p.1011, 1970.

[10] A. Al-Omar and J. P. Krusius, COMPEL, vol.6, p. 3, 1987.